RSC Advances

PAPER

View Article Online
View Journal | View Issue

Cite this: *RSC Adv.*, 2023, **13**, 8101

Gold and palladium supported on an ionic liquid modified Fe-based metal–organic framework (MOF) as highly efficient catalysts for the reduction of nitrophenols, dyes and Sonogashira–Hagihara reactions†‡

Shirin Karimi,[a] Mohammad Gholinejad, *[ab] Rahimeh Khezri,[c] José M. Sansano,[de] Carmen Nájera[e] and Miguel Yus[e]

Received 14th January 2023
Accepted 1st March 2023

DOI: 10.1039/d3ra00283g

rsc.li/rsc-advances

Two supported noble metal species, gold and palladium anchored on an ionic liquid-modified Fe-based metal–organic framework (MOF), were successfully synthesized and characterized by FT-IR, XRD, TEM, XPS, SEM, EDX, and elemental mapping. The ionic liquid post-modified MOF was used for anchoring Au or Pd at ppm levels, and the resulting materials were employed as catalysts in the reduction of nitrophenol isomers, dyes, and Sonogashira–Hagihara reactions. Using the Au@Fe-MOF-IL catalyst, reduction of nitrophenol isomers, as well as the reductive degradation of dyes, *e.g.*, methylene blue (MB), methyl orange (MO), and methyl red (MR) were performed efficiently in water. On the other hand, Pd@Fe-MOF-IL was used as an effective catalyst in the Sonogashira–Hagihara coupling reaction of aryl iodides and bromides using very low amounts of Pd. These catalysts were recycled and reused for several runs without deteriorating remarkably in catalytic performance.

1. Introduction

Coordination polymers or metal–organic frameworks (MOFs) are a unique class of ultra-porous crystalline materials composed of inorganic nodes containing metal ions/clusters and rods constructed by polydentate organic linkers through robust bonds. MOFs, with special properties and applications, can be designed rationally by applying different metal nodes (intermediate/non-intermediate) and various organic linkers (carboxylate, phenolate, azolate, sulfonate, *etc.*). These materials with permanent porosity, inherent crystallinity, flexible structures, and high specific surface areas have been shown to have potential applications in gas molecules storage and separation (such as H_2, CO_2, N_2, C_2H_2, CH_4, *etc.*), as sensors, as ion conductors, for drug delivery, as supercapacitors, or for catalysis.[1–8] In recent years, numerous studies have been conducted on the use of MOFs as heterogeneous catalysts in various reactions, such as the Knoevenagel condensation reaction,[9] epoxide ring opening,[10] and oxidation.[11] Recently, an extensive study has also been done on post-synthetic modification of MOFs.[12–14] Additionally, extensive study has been developed on the post-synthetic modification of MOFs in which it is possible to adjust the chemical properties of the walls of the channels using organic linkers, and also modifying MOFs external surface using different functional groups. By using these modifications, MOFs with the same topology, but different functional groups, can be produced.[12–14] Along this line, covalent post-synthesis modification of MOFs with ionic liquids is an effective method to improve the stability of MOFs and provides the possibility of stabilizing different types of transition metals and nanoparticles (NPs).[15] The introduction of metal nanoparticles in these structures drives the creation of bimetallic systems, which brings the synergistic effect of the metal nanoparticles introduced with the metal nodes in the MOF structure and enhances the catalytic activity.[16–18]

Nowadays, the increasing use of organic pollutants in industry and agriculture and the removal of these pollutants from the environment has become a severe concern for the environment and scientists.[19–21] Among them, dyes and

[a]*Department of Chemistry, Institute for Advanced Studies in Basic Sciences (IASBS), P. O. Box 45195-1159, Gavazang, Zanjan 45137-66731, Iran. E-mail: gholinejad@iabs.ac.ir*

[b]*Research Center for Basic Sciences & Modern Technologies (RBST), Institute for Advanced Studies in Basic Sciences (IASBS), Zanjan 45137-66731, Iran*

[c]*Department of Chemistry, Faculty of Sciences, Persian Gulf University, Bushehr, 75169, Iran*

[d]*Departamento de Química Orgánica, Instituto de Síntesis Orgánica, Universidad de Alicante, Apdo. 99, 03690-Alicante, Spain*

[e]*Centro de Innovación en Química Avanzada (ORFEO-CINQA), Universidad de Alicante, Apdo. 99, 03690-Alicante, Spain*

† Dedicated with honour to Prof. Irina Beletskaya on the occasion of her 90th anniversary.

‡ Electronic supplementary information (ESI) available. See DOI: https://doi.org/10.1039/d3ra00283g

nitrophenols are extensively used in various industries, such as food industries, textile, papermaking, painting, beauty, explosives, leather, rubbers, pulp, paper industries, printing, pharmaceuticals, *etc.* These compounds are considered as main hazardous pollutants[22–25] which exposure them even for a short time leads to problems such as eye irritants, skin and breathing issues, cough, kidney and liver damage, lung diseases, cancer, *etc.* Many nitrophenols and dyes were listed as pollutants in European legislation on textile dyeing and United States environmental legislation.[26–30] In this regard, the approach of catalytic chemical reduction in which these toxic compounds are converted into substances with less toxicity or even valuable products has attracted the attention of many scientists.[31–36]

Sonogashira–Hagihara coupling reaction between vinyl or aryl halides and terminal alkynes generated conjugated enynes and aryl alkynes, which are important functional groups in polymers, natural products, pharmaceuticals, materials science, *etc.*[37–42]

Different organic reactions can be efficiently catalyzed by precious metals. In the past, these metals were used at mol% concentrations in various reactions, which possess serious problems due to their limited resources and high price. Research today focuses on the efficiency and biocompatibility of reactions. This can be achieved by reducing the total reaction volume, changing the (pre)catalyst (including its engineering and designing cost-effective ones), or reducing its quantity. Along this line, some studies have been reported high catalytic activity using noble metals under ppm levels.[43–45] For instance, previous reports indicated that the trace amount of contaminants in $FeCl_3$ plays a significant role in the success of different organic reactions including Sonogashira–Hagihara reaction.[46,47] Subsequently, from the vast number of MOF frameworks reported in the literature, we selected Fe-based MOF, NH_2-MIL-88B(Fe), and its ionic liquid modified was used for anchoring Au and Pd noble metal species at the ppm levels (Au@Fe-MOF-IL and Pd@Fe-MOF-IL). Au@Fe-MOF-IL showed excellent catalytic activity in reduction of nitrophenols isomers and structurally different organic dyes, and Pd@Fe-MOF-IL was successfully applied in Sonogashira–Hagihara coupling reactions of aryl bromides and iodides.

2. Results and discussion

2.1. Synthesis and characterization of Au@Fe-MOF-IL (3) and Pd@Fe-MOF-IL (4)

NH_2-MIL-88B(Fe) MOF **1** was synthesized *via* the reaction of $FeCl_3 \cdot 6H_2O$ and 2-aminoterephthalic acid at 150 °C (Scheme 1a).[17] On the other hand, **IL** was obtained by reacting 1-methyl imidazole and 1,2-dibromoethane in dry THF (Scheme 1b). As outlined in Scheme 1c, NH_2–Fe MOF modified ionic liquid was easily synthesized *via* NH_2–Fe-MOF (**1**) reaction with **IL** in the presence of Et_3N as a base. Au and Pd metals were anchored on Fe-MOF-IL material through the reaction of $HAuCl_4 \cdot 3H_2O$ and $PdCl_2$ solutions with MOF (**2**), respectively (Scheme 1d). In the case of Au@Fe-MOF-IL, final material was achieved after treating with $NaBH_4$.

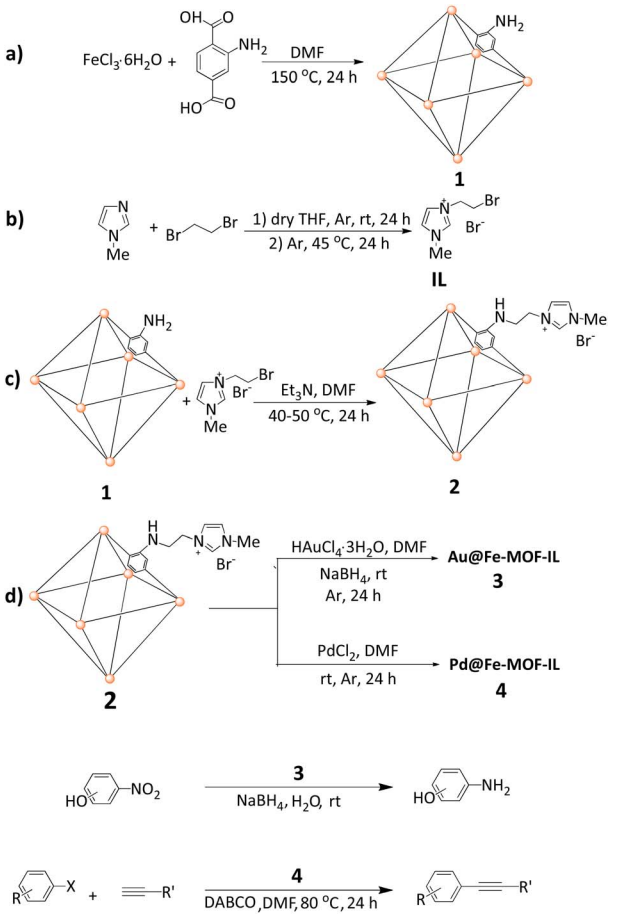

Scheme 1 Synthesis of Au@Fe-MOF-IL and Pd@Fe-MOF-IL and their application as catalyst.

The structure of as-prepared samples characterized by FT-IR, TEM, SEM, XPS, XRD, and EDX, elemental mapping analysis. The chemical groups of all samples were determined by FT-IR spectrum, in the range of 400–4000 cm^{-1}, and the results were given in Fig. 1. The observed peaks at 768 cm^{-1} stand assigned to the vibration peak of C–H, due to the benzene ring,[42] while the band at 1255 cm^{-1} refers to stretching vibrations of C–N group.[48,49] A broad peak, at 2970 cm^{-1} can be attributed to the 2-aminoterephthalic acid ligand, resulting from the existence of the –OH group.[50] Therefore, the disappearance of –OH stretching vibration peaks confirmed the synthesis of Fe-MOF due to coordination between the target metals and the –COOH group of 2-aminoterephthalic acid. Also, the absorption bands at 1578 and 1381 cm^{-1}, can be attributed to the symmetric and asymmetric stretching of C–O of the carboxylate group.[51] Two peaks observed at 3130 and 2927 cm^{-1} distinguish the asymmetric and symmetric vibration of the amino groups.[52] The observed peaks at 3460 and 3334 cm^{-1} are related to N–H in addition, the peak at ~1651 cm^{-1} stands related to CONH bands resulting from coordinated the residual DMF.[53] Results indicated the overlap of the characteristic peak of C–N and C=C bonds at ~1650 cm^{-1} in imidazole ring with CONH peak.[54,55]

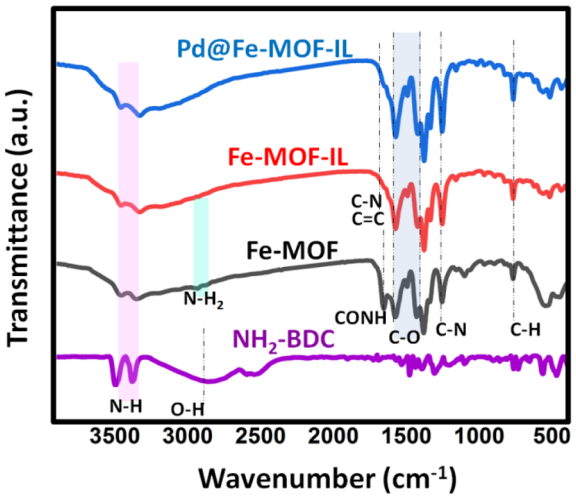

Fig. 1 IR spectrum of Fe-MOF-IL, Au@Fe-MOF-IL and Pd@Fe-MOF-IL.

As shown in Fig. S1,‡ X-ray diffraction (XRD) measurements confirmed the crystalline structures of Fe-MOF-IL, Au@Fe-MOF-IL, and Pd@Fe-MOF-IL. Fe-MOF-IL exhibits similar diffraction patterns to those reported in previous literature, with strong peaks at 9.2° and 10.2°, which correspond to (002) and (101).[56–58]

The similar XRD pattern observed for Au@Fe-MOF-IL, and Pd@Fe-MOF-IL, suggest that the immobilization of Au and Pd did not cause an obvious change in the crystallinity of Fe-MOF-IL. Due to the low content of Au and Pd, no diffraction peaks related for these metals were observed. However, their existence was confirmed, by other analyses, including atomic absorption spectroscopy. The Au and Pd contents in the composites were determined as 0.43 mmol g^{-1} and 0.49 mmol g^{-1}, respectively.

The newly-formed chemical bonds within the prepared catalysts were characterized by XPS analysis. Apart from Fe 2p, O 1s, N 1s, and C 1s, the appearance of Au 4f and Pd 3d signals for Au@Fe-MOF-IL and Pd@Fe-MOF-IL further confirmed the loading of Au and Pd in them, respectively (Fig. 2). It should be noted peaks at 711.3, and 725.5 eV are associated with Fe^{3+} $2p_{3/2}$ and Fe^{3+} $2p_{1/2}$. Whereas the peaks at 710.7 and 723.4 eV are related to Fe^{2+} $2p_{3/2}$ and Fe^{2+} $p_{1/2}$ (Fig. 2b and i).[59] N 1s spectra of functionalized MOFs were divided into three symmetrical peaks, and evidence was observed in Fig. 2f and k. The B.E. centered at 399 eV, 400.7 eV, and 401.4 eV were related to N–C, N–H, and $^{+}$N=C–, respectively.[60,61]

These results proved successful post-synthetic modifications of organic linkers with ionic liquid. In addition, XPS results proved Fe-MOF-IL coordination with Au(0), Au(I) and Pd(II), for the Au@Fe-MOF-IL and Pd@Fe-MOF-IL catalysts, respectively. Two pair peaks at 83.4, 87.2 eV and 85.1, 88.6 eV were showing existence of two oxidation state (0) and (I) for Au in Au@Fe-MOF-IL (Fig. 2a). Also peaks at 338 and 343.1 eV, indicated existence of Pd(II) in Pd@Fe-MOF-IL (Fig. 2g).[59,62]

The morphology of the Fe-MOF-IL, Au@Fe-MOF-IL and Pd@Fe-MOF-IL were investigated by the scanning electron microscopy (SEM) and transmission electron microscopy (TEM). The immobilized Au NPs have a ~13 nm average size (Fig. S3‡). The corresponding evidence showed that desired catalysts pointing to two types of morphology, including decorated with small irregularly shaped particles and spindle morphology. TEM images of the prepared MOFs also confirm the presence of irregularly-shaped particles, in addition to the

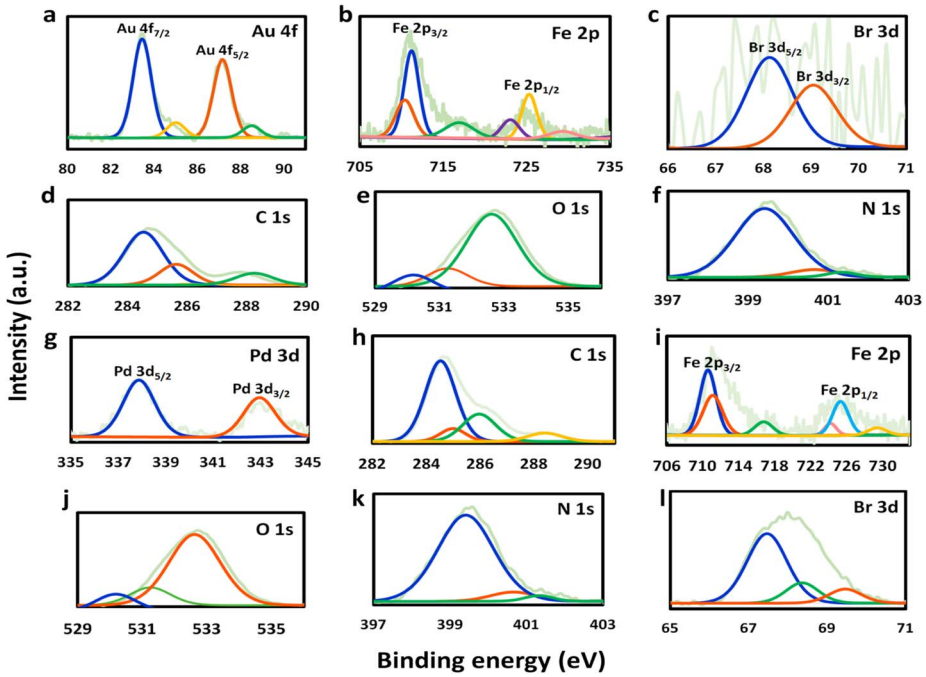

Fig. 2 XPS analysis of Au@Fe-MOF-IL from (a) Au, (b) Fe, (c) Br, (d) C, (e) O and (f) N, and XPS analysis of Pd@Fe-MOF-IL from (g) Pd, (h) C, (i) Fe, (j) O, (k) N and (l) Br.

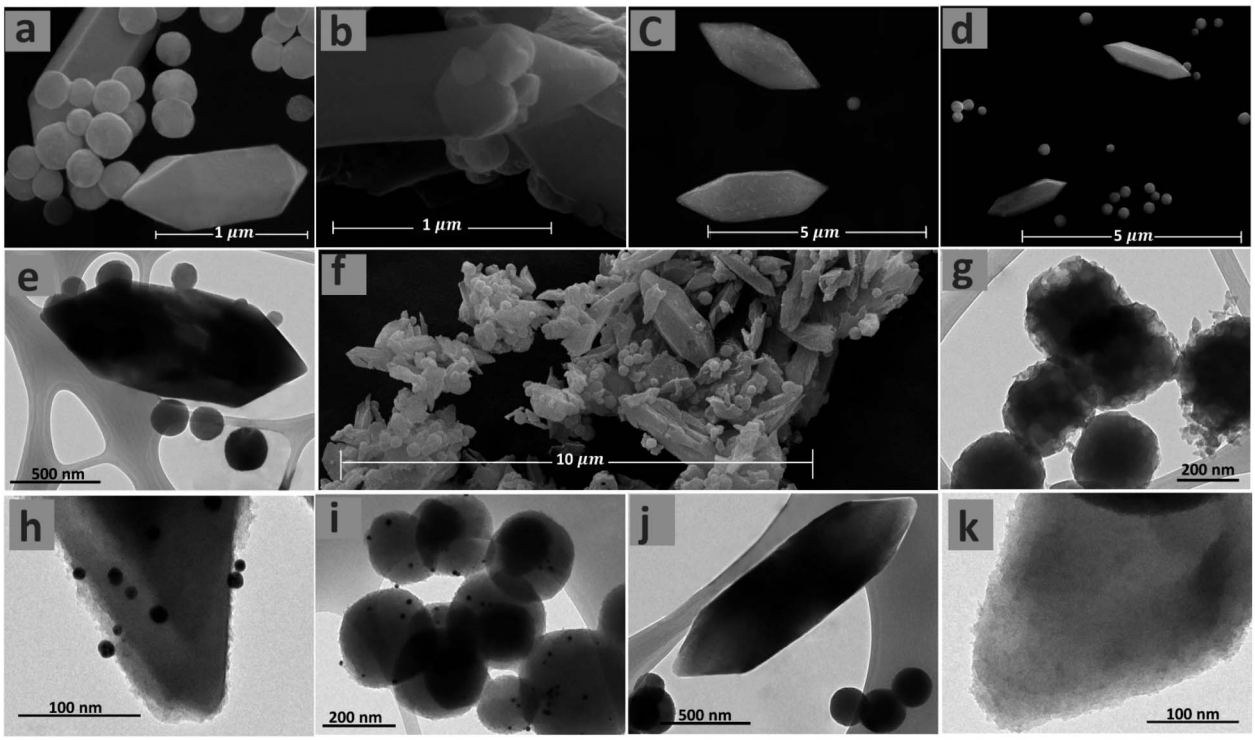

Fig. 3 SEM images of Fe-MOF-IL (a, b and f), Au@Fe-MOF-IL (c), and Pd@Fe-MOF-IL (d). TEM images of Fe-MOF-IL (e and g), Au@Fe-MOF-IL (h and i) and Pd@Fe-MOF-IL (j and k) in different magnification.

spindle-shaped morphology shown in the SEM images (Fig. 3). Scanning electron microscopy (SEM) and TEM measurements indicate that the immobilization of Au and Pd particles did not alter the morphology of Fe-MOF-IL support.[63]

Thermogravimetric analysis (TGA) profiles of the obtained samples are present in (Fig. S2‡). TGA curves show that the weight loss took place in three regions. The first weight loss of Fe-MOF, Fe-MOF-IL, Au@Fe-MOF-IL, and Pd@Fe-MOF-IL, were *ca.* 2 wt%, 11 wt%, and 8 wt% at 40–134, 40–258, and 40–230 °C in the diagram, respectively. This weight loss was related to the loss of the solvent molecules from their pores. Their most mass loss was the second step which corresponded to the loss of organic linkers. It should be noted increasing weight loses in Fe-MOF-IL, Au@Fe-MOF-IL, and Pd@Fe-MOF-IL compared to Fe-MOF is results of successful attachment of **IL** to MOF structure. The complete decomposition of Fe-MOF, Fe-MOF-IL, Au@Fe-MOF-IL, and Pd@Fe-MOF-IL, occurred at ~440 °C with 45%, 70%, 67%, and 65% mass loss, respectively (Fig. S2‡).

Energy dispersive X-ray spectroscopy (EDX) analyses and elemental mapping images confirmed the presence of different elements as well as Au and Pd in Au@Fe-MOF-IL and Pd@Fe-MOF-IL, respectively (Fig. 4 and 5).

2.2. Catalytic performance of Au@Fe-MOF-IL for nitrophenol isomers reduction

We evaluated the catalytic activity of synthesized Au@Fe-MOF-IL catalyst for nitrophenol isomers reductions. To find optimized conditions, effect of several parameters including the type of reducing agent and its amount, catalyst loading (mol%), type of solvent, and required time for performing the reaction was investigated in reduction of *p*-nitrophenol as a model compound. Initially, the reaction of *p*-nitrophenol and 4 equiv.

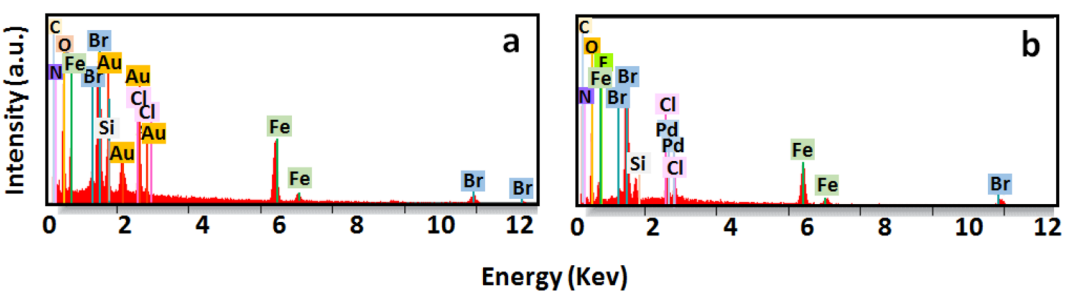

Fig. 4 EDX analysis of Au@Fe-MOF-IL, and Pd@Fe-MOF-IL.

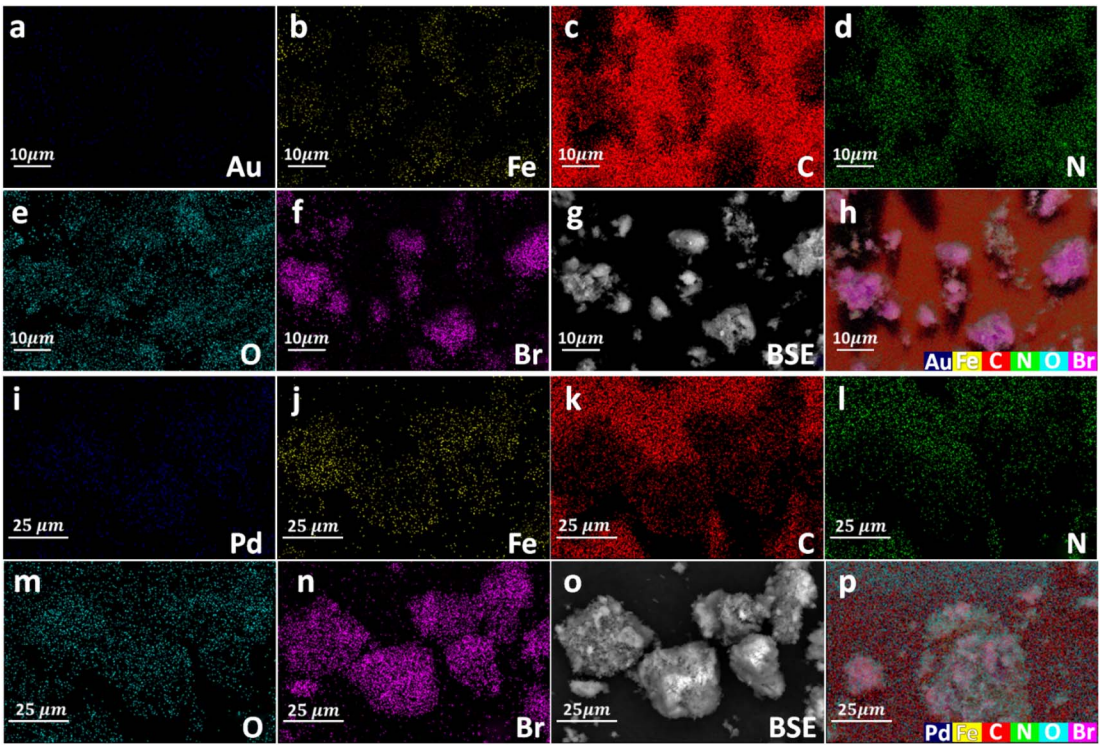

Fig. 5 Elemental mapping images of Au@Fe-MOF-IL (a–h), and Pd@Fe-MOF-IL (i–p).

of $NaBH_4$ were conducted using 0.054 mol% of catalyst in a mixture of H_2O/EtOH solvents at room temperature for 15 min (Table 1, entry 1). By reducing the amount of catalyst to 0.033 mol%, there was no change in the reaction efficiency (Table 1, entry 3), however, further reducing the amount of catalyst to 0.027 mol% resulted in a decrease in the reaction yield (Table 1, entry 4). Then, the reduction of 4-nitrophenol was tested in water as the reaction solvent. In this condition, the reaction yield was decreased negligible (1%), which was ignored due to the significant advantage of the water (*e.g.* being environmentally friendly) (Table 1, entry 5). The amounts of $NaBH_4$ were subsequently decreased to 3 and 2 equiv., respectively, which led to a decrease in produced 4-aminophenol yields (Table 1, entries 7 and 8, respectively). Results demonstrated that 4-aminophenol could be obtained in excellent yield (100%), by using 4 equiv. of $NaBH_4$. When the reaction time was reduced to 10 min, lower yields were observed (Table 1, entry 9). To show the synergistic effect, between the metals present in the prepared MOF, reduction of 4-nitrophenol was performed with MOF material (Table 1, entries 2 and 6), which resulted in a lower yield. Different reducing agents *e.g.*, glycerol, formic acid, and hydrazine were also examined for the reduction of 4-nitrophenol, in all cases providing poor yields as compared to $NaBH_4$ (Table S1, entries 1–4‡). Gratifyingly, we found that for efficient reduction of nitrophenol, 0.033 mol% catalyst (4.3 ppm), 4 equiv. $NaBH_4$ in water as solvent at room temperature is required.

Upon reaction optimization, the catalytic reduction of two other nitrophenol isomers (*m*-nitrophenol and *o*-nitrophenol) were subsequently investigated. The yields of the catalytic reduction for *o*-, and *m*-nitrophenol were 99% and 94%, respectively (Table 2, entries 1 and 2).

In addition to catalyst activity, its reusability is a significant point in practical application. To aim of investigate its recovery performance, Au@Fe-MOF-IL was examined by successive

Table 1 Optimization of the reduction of 4-nitrophenol at room temperature[a]

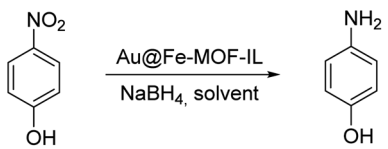

Entry	Au (mol%)	$NaBH_4$	Solvent	t (min)	Yield[b] (%)
1	0.054	4 equiv.	H_2O/EtOH (1 : 1)	15	100
2	0.054	4 equiv.	H_2O/EtOH (1 : 1)	15	37[c]
3	0.033	4 equiv.	H_2O/EtOH (1 : 1)	15	100
4	0.027	4 equiv.	H_2O/EtOH (1 : 1)	15	90
5	0.033	4 equiv.	H_2O	15	99
6	0.033	4 equiv.	H_2O	15	44[c]
7	0.033	3 equiv.	H_2O	15	90
8	0.033	2 equiv.	H_2O	15	90
9	0.033	4 equiv.	H_2O	10	85

[a] Reaction conditions: 4-nitrophenol (0.5 mmol) and solvent (3 mL) in 5 mL reaction tube stirred for desire time. [b] The yield was determined by gas chromatography (GC). [c] Use of metal-free Fe-MOF as catalyst.

Table 2 Reduction reactions of nitrophenol isomers[a]

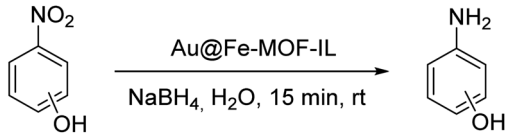

Entry	Nitrophenol	Product	Yield[b] (%)
1	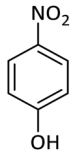	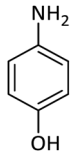	99
2	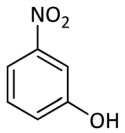	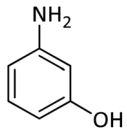	99
3	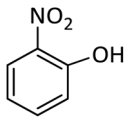	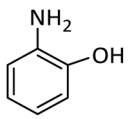	94

[a] Reaction conditions: 4-nitrophenol (0.5 mmol), $NaBH_4$ (2 mmol), catalyst (0.003 mol% Au, 2.1 mol% Fe, 6 mg) and solvent (3 mL) in 5 mL reaction tube stirred for desire time. [b] The Yield was determined by gas chromatography (GC).

cycles of catalytic reduction reactions. In a typical experiment, the catalyst was isolated from an as-completed reaction solution and used directly for the next reaction cycle. Results of these studies exhibited that catalyst could successfully have recycled and reused for 9 sequential runs without diminution in catalytic activity. However, in run 10, the yield of the corresponding product quickly declined to 81% (Fig. S4‡).

2.3. Catalytic performance of Au@Fe-MOF-IL for nitrophenol isomers reduction studied by UV-vis

In addition, the catalytic performance of the Au@Fe-MOF-IL was also evaluated using nitrophenol isomers catalytic reduction investigated *via* UV-vis spectroscopy. When $NaBH_4$ without the catalyst was added into the target solutions, the peak intensities of 4-NP, 3-NP, and 2-NP at around 401, 393, and 415 nm respectively, do not change clearly after 30 min, which indicates that presence of Au@Fe-MOF-IL catalyst is necessary for the reduction of nitrophenol isomers (Fig. S5‡).[64] On the other hand, the reaction in the presence of MOF without Au particles led to partial conversion (~50%), which confirms the synergistic effect of the substrate with Au particles (Fig. S5‡). Nevertheless, the Fe-MOF-IL anchored Au particles efficiently promote the reduction reaction of nitrophenol isomers by $NaBH_4$. In the presence of Au@Fe-MOF-IL, the characteristic peak intensity of nitrophenol gradually was decreased with the progress of the reaction time, while the characteristic peak intensity of aminophenol increased (Fig. 6). In the 4-NP, 3-NP,

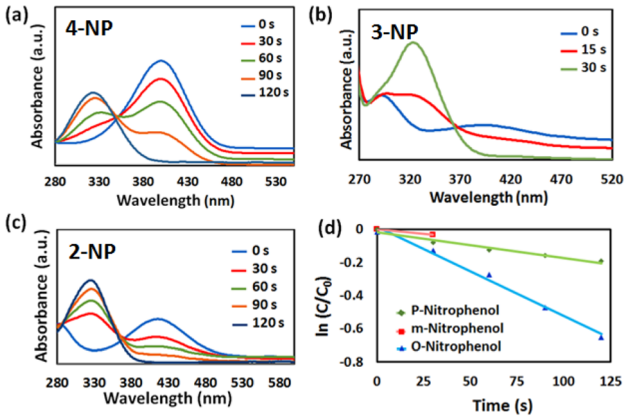

Fig. 6 UV-vis absorption spectra of (a) 4-nitrophenol (b) 3-nitrophenol (c) 2-nitrophenol reduction with Au@Fe-MOF-IL in the presence of $NaBH_4$. (d) Plot of $\ln(C/C_0)$ *versus* reaction time derived from spectra showed in (a)–(c).

and 2-NP reduction experiments, the complete reduction indicates producing the desired products in 100%, 96%, and 97% conversion with Au@Fe-MOF-IL catalyst after 120 s, 30 s, and 120 s, respectively. These conversions calculate using the UV-visible spectra (where C_0 and C_t are the absorbance of nitrophenol at initial concentration and nitrophenol concentration at time t, respectively):

$$\text{Conversion}\% = \frac{C_0 - C_t}{C_0} \times 100 \quad (1)$$

In addition, the reaction apparent rate constant also was calculated according to the relationship between $\ln(C/C_0)$ and reaction time (where k (s^{-1}) is the kinetic rate constant, C_0 and C_t are the absorbance of nitrophenol at initial concentration and nitrophenol concentration at time t, respectively, and t (s) indicate reaction time):

$$\ln(C_0/C_t) = -kt \quad (2)$$

The apparent rate constant (k_{app}) of the as-prepared Au@Fe-MOF-IL was 5.4×10^{-3} s^{-1}, 3.3×10^{-3} s^{-1} and 1.6×10^{-3} s^{-1} in reduction of 4-NP, 3-NP and 2-NP respectively which was calculated based on eqn (1) and Fig. 6d.[65] According to Fig. 6d and 7d, a linear correlation between the $\ln(C_t/C_0)$ and the reaction time is observed. However, it represents pseudo-first-order kinetics, due to the excess $NaBH_4$. These results clearly show the effective catalytic activity of Au@Fe-MOF-IL in the reduction reaction of nitrophenol isomers. As evident, the reduction of *m*-nitrophenol was immediate. In contrast, the reduction reaction of *p*-nitrophenol and *o*-nitrophenol isomers occurred during higher times. This difference in reactivity attributes to the higher basicity nature of the *m*-nitrophenol isomer. However, the conjugation effect delocalized the negative charge of *p*-nitrophenolate and *o*-nitrophenolate ions and led to the positivity of the nitrogen atom. This reason can explain two other isomers lower activity.

2.4. Catalytic performance of Au@Fe-MOF-IL for dyes reduction reaction studied by UV-vis

The catalytic activities of Au@Fe-MOF-IL for the reduction of toxic organic dyes (MB, MO and MR) were also evaluated in the presence of $NaBH_4$. The progress of the reduction reactions was monitored *via* UV-vis spectroscopy. When Au@Fe-MOF-IL with $NaBH_4$ puts into the target solutions, the absorbance of MB ($\lambda_{max} = 464$ nm), MO ($\lambda_{max} = 460$ nm), and MR ($\lambda_{max} = 435$ nm) slowly decreases with increasing reaction time (Fig. 7).[65–67] The apparent rate constant (k_{app}) of 1.46×10^{-2} s^{-1}, 5.6×10^{-3} s^{-1}, and 7×10^{-3} s^{-1}, were obtained for the reduction reaction of MB, MO, and MR catalyzed by Au@Fe-MOF-IL.

2.5. Catalytic performance of Pd@Fe-MOF-IL for Sonogashira–Hagihara alkynylation coupling

Catalysts based on palladium indicated effective catalytic activity in the Sonogashira–Hagihara coupling reaction.[68] Thus, the catalytic activity of Pd@Fe-MOF-IL was evaluated in the Sonogashira–Hagihara coupling reaction of aryl halides with terminal alkynes. To achieve optimal conditions, we chose the reaction of iodobenzene with phenylacetylene as the reaction model. To achieve this goal, various parameters such as catalyst loading, type of base, solvent, and reaction temperature were examined (Table 3). The condition including 0.15 mol% Pd loading in DMSO solvent and NaOAc base at 80 °C revealed relatively good yields (Table 3, entry 1). It was observed that desired product, 1,2-diphenylethyne in good yield was obtained in DMF in comparison with the other solvents (Table 3, entries 2–7). The influence of bases on the Sonogashira coupling reaction was also examined, DABCO served as the most suitable bases among the different studied bases for this reaction (Table 3, entries 8–12). According to the results, the amount of palladium as an important factor in this reaction was investigated. It was observed that 12.5 mg Pd@Fe-MOF-IL containing 0.05 mol% Pd loading was chosen as the most appropriate (Table 3, entries 12–15). As presented in Table 3, entry 16, the model reaction performed without Pd (blank runs), under optimum conditions, produced desired product just in 18% yield. Next, the effect of temperature was examined to explore

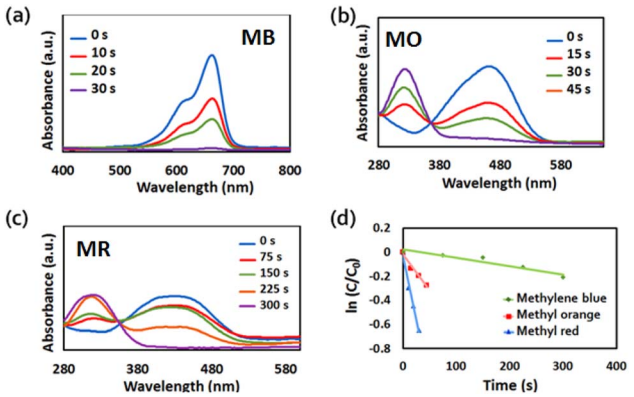

Fig. 7 UV-vis absorption spectra of (a) MB (b) MO (c) MR reduction with Au@Fe-MOF-IL in the presence of $NaBH_4$. (d) Plot of $\ln(C/C_0)$ *versus* reaction time derived from spectra showed in (a)–(c).

Table 3 Reaction conditions optimization for cross-coupling of phenyl acetylene and iodobenzene catalyzed by Pd@Fe-MOF-IL[a]

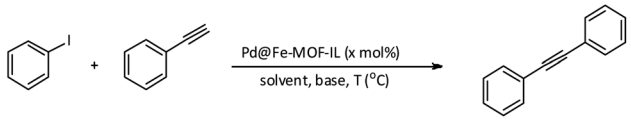

Entry	Catalyst (mol% Pd)	Base	Solvent	T (°C)	Yield[b] (%)
1	0.15	NaOAc	DMSO	80	73
2	0.15	NaOAc	DMF	80	76
3	0.15	NaOAc	CH_3CN	80	13
4	0.15	NaOAc	1,4-Dioxane	80	10
5	0.15	NaOAc	Toluene	80	6
6	0.15	NaOAc	H_2O	80	48
7	0.15	NaOAc	H_2O : EtOH	80	55
8	0.15	DABCO	DMF	80	97
9	0.15	Na_3PO_4	DMF	80	86
10	0.15	K_2CO_3	DMF	80	21
11	0.15	Et_3N	DMF	80	14
12	0.15	$NaNO_3$	DMF	80	10
13	0.10	DABCO	DMF	80	97
14	0.05	DABCO	DMF	80	96
15	0.03	DABCO	DMF	80	72
16	—	DABCO	DMF	80	18
17	0.05	DABCO	DMF	60	81
18[c]	0.05	DABCO	DMF	80	63

[a] Reaction conditions: iodobenzene (0.5 mmol), phenylacetylene (0.75 mmol), base (0.75 mmol) in solvent (2 mL), 24 h. [b] GC yields. [c] Reaction times: 18 h.

the best condition for the reaction. It was observed that the reaction temperature also plays a crucial role in the reaction yield. Decreasing the reaction temperature to 60 °C has resulted in a lower yield of desired product (Table 3, entry 17). Moreover, we attempted to examine the time dependence of the catalyst on the coupling reaction, due to the reaction time dropped to 18 h, the yields decreased to 63% (Table 3, entry 18).

In the next step, following the optimal reaction conditions, we further expanded the scope of the Sonogashira–Hagihara reaction for the reaction of a series of alkenes with a wide range of electron-withdrawing or electron-donating aryl halides. As shown in Table 4 aryl iodide as well as both of its electron-donating (*e.g.*, $-CH_3$, and $-OCH_3$) and electron-withdrawing substituents (such as, –CHO, $-NO_2$, –CN, and –Cl) were able to provide the desired products in excellent yields (Table 4, entries 1–9). Furthermore, coupling reaction of heteroaromatic including 2-iodothiophene with alkynes gave the desired product in excellent yields (Table 4, entries 10–12). As observed in entries 12 and 13 propargyl alcohol yielded the desired product in excellent yields (Table 4, entries 12 and 13). Due to these results, we examined the catalytic activity of Pd@Fe-MOF-IL in the Sonogashira coupling reaction of phenylacetylene with various aryl and heteroaryl bromides. Fortunately, aryl bromides with electron-withdrawing substituents such as $-NO_2$, –CHO, and –CN also obtained products in excellent yields (Table 4, entries 14–16). Furthermore, the reaction of phenylacetylenes with heterocyclic bromides such as 2-bromopyridine

Table 4 Sonogashira–Hagihara reaction of various types of aryl iodides[a] and aryl bromides[b] with alkynes catalyzed by Pd@Fe-MOF-IL

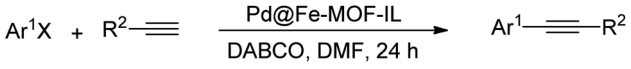

Entry	Aryl halide	Alkyne	Product	Yield[c] (%)
1	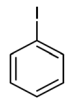	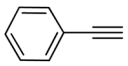	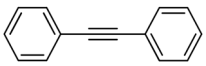	96
2	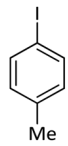	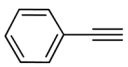	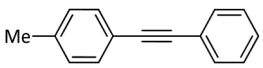	91
3	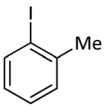	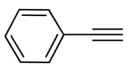	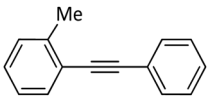	93
4	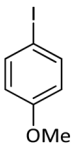	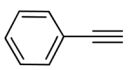	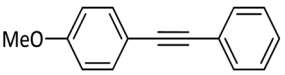	95
5	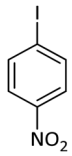	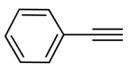	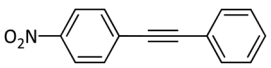	94
6	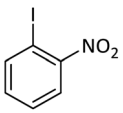	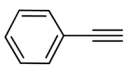	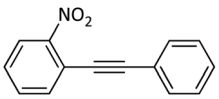	97
7	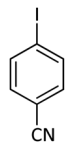	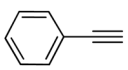	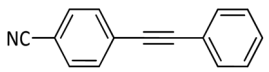	90
8	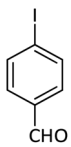	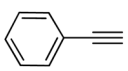	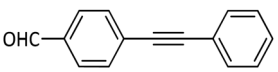	92
9	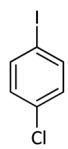	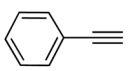	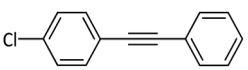	89
10		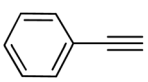	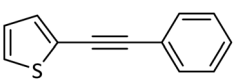	98
11		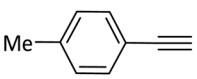	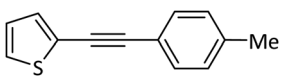	94
12		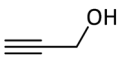	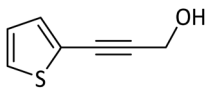	91

Table 4 (*Contd.*)

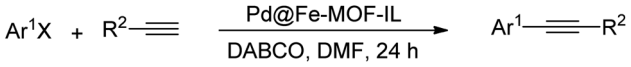

Entry	Aryl halide	Alkyne	Product	Yield[c] (%)
13	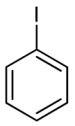	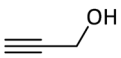	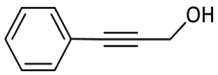	98
14	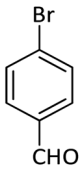	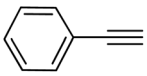	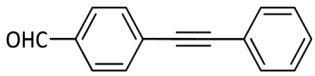	88
15	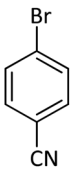	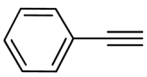	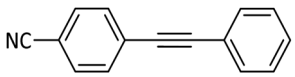	90
16	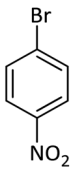	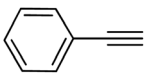	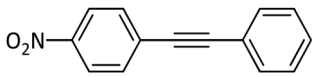	93
17	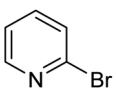	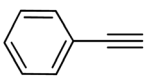	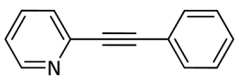	84
18	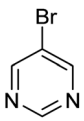	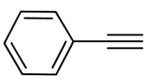	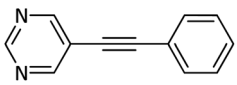	89
19	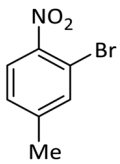	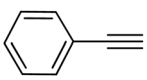	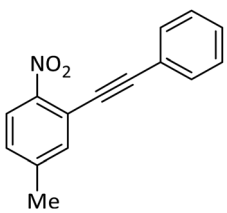	78

[a] Reaction conditions for coupling reaction of aryl iodides: ArI (0.5 mmol), alkyne (0.75 mmol), DABCO (0.75 mmol), catalyst (0.05 mol% Pd, 12.5 mg) and DMF (2 mL) at 80 °C. [b] Reaction conditions for coupling reaction of aryl bromides: ArBr (0.5 mmol), alkyne (0.75 mmol), DABCO (0.75 mmol), catalyst (0.11 mol% Pd, 25 mg) and DMF (2 mL) at 80 °C. [c] GC yields.

and 5-bromopyrimidine yielded corresponding products in 84% and 89% yield, respectively (Table 4, entries 17 and 18). Aryl chlorides reaction was also examined but results indicated that under optimized reaction conditions reactions did not proceed well.

The heterogeneous nature of Pd@Fe-MOF-IL in the Sonogashira–Hagihara reaction of phenylacetylene with iodobenzene was also evaluated by the filtration test. For this purpose, the catalyst was taken out after 2 h, which was bring yielded 25%. Then, filtrate was allowed to further react for 22 h under optimized condition. GC result indicated formation of desire product in 50% confirming almost heterogeneous nature of catalyst. The reusability of Pd@Fe-MOF-IL, was also investigated by successive cycles of catalytic reactions in the Sonogashira–Hagihara coupling reaction (Fig. 8). A typical experiment involves isolating the catalyst from a completed reaction

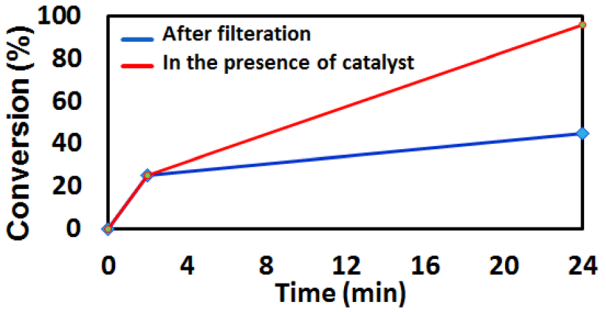

Fig. 8 Filtration test of Pd@Fe-MOF-IL in the Sonogashira–Hagihara reaction.

solution and using it directly for a new reaction cycle. The results of these examinations confirmed that the catalyst could be successfully recycled and reused for 5 sequential runs without diminution in catalytic activity. However, from run 6, the yield of the corresponding product quickly declined to 61% (Fig. S6‡).

3. Conclusions

The two gold and palladium supported catalysts easily prepared by anchoring an imidazolium unit to the Fe-based MOF allowed a very low loading of nanoparticles at ppm levels. For the reduction of organic pollutants using $NaBH_4$ such as nitrophenols, Au@Fe-MOF-IL showed a high catalytic efficiency and high recyclability. In addition, toxic organic dyes such as methylene blue, methyl orange and methyl red can be removed from water. For the Sonogashira–Hagihara reaction, Pd@Fe-MOF-IL works as catalyst with very low Pd loading in DMF at 80 °C for the cross-coupling of terminal acetylenes with aryl iodides and bromides. Recycling experiments showed that this supported catalyst can be recycled and reused during five cycles. Synergistic effects between Fe and Au or Fe and Pd are important in catalytic activities in reduction and in Sonogashira–Hagihara reactions, respectively.

4. Experimental section

4.1. General methods

Tetrachloroauric(III) acid trihydrate ($HAuCl_4 \cdot 3H_2O$, 99.5%), palladium chloride ($PdCl_2$, ≥99.9%), iron(III) chloride hexahydrate ($FeCl_3 \cdot 6H_2O$, 99%), 2-aminoterephthalic acid (NH_2–BDC, 99%), nitrophenol isomers, sodium borohydride ($NaBH_4$), aryl halides, phenylacetylene, *N*,*N*-dimethylformamide (DMF, 99.9%), methyl orange (MO), methyl red (MR), and methylene blue (MB) were purchased from Merck Millipore-Sigma, Sigma-Aldrich, and Acros. ^{13}C NMR and ^{1}H NMR spectra were conducted at 100 MHz and 400 MHz, respectively on Bruker Avance HD. Chemical shifts are set on the δ-scale in ppm, and residual solvent peaks were utilized as internal standards. X-ray diffraction (XRD) patterns performed using Philips X'Pert Pro instrument. The SEM and TEM analyses were taken by JEOL JSM 840 and EOL JEM-2010, respectively. X-ray detector Bruker XFlash 3001 applied with SEM equipment for microanalysis (EDS) and mapping. XPS analyses were achieved by K-Alpha spectrometer.

4.2. Synthesis of NH_2-MIL-88B(Fe) MOF

The NH_2-MIL-88B(Fe) MOF was synthesized according to the modified solvothermal method previously reported in our group.[17] 2-Aminoterephthalic acid (3 mmol, 0.54 g) and $FeCl_3 \cdot 6H_2O$ (3 mmol, 0.81 g) were dissolved in DMF (67 mL). The resulting solution was stirred for 20 min at room temperature and then sonicated for 15 min. Afterwards, the solution was transferred into a 100 mL Teflon-lined autoclave and heated at 150 °C for 24 h. The brown precipitate was separated using centrifugation, washed with DMF and absolute ethanol three times, then dried in a vacuum oven at 50 °C for 24 h.

4.3. Synthesis of 1-(2-bromoethyl)-3-methylimidazolium bromide ionic liquid (IL)

1,2-Dibromoethane (5 mmol), 1-methyl imidazole (2 mmol), and dry THF (1 mL) were added to a 10 mL container and stirred continuously at room temperature for 24 h under argon atmosphere. Then, the mixture was gradually heated up to 45 °C, and the reaction persisted for another 24 h. The resulting pale-yellow precipitate was washed three times with *n*-hexane and dried at 50 °C for 24 h. ^{1}H NMR (DMSO, 400 MHz) δ (ppm): 9.34 (s, 1H), 7.91 (s, 1H), 7.82 (s, 1H), 4.67 (2H, t, $J = 6$), 3.99 (2H, t, $J = 6$), 3.93 (s, 3H); ^{13}C NMR (DMSO, 101 MHz) δ (ppm): δ ^{13}C NMR (101 MHz, DMSO) δ 137.6, 137.4, 124.3, 124.2, 122.9, 122.8, 50.5, 36.5, 36.3, 32.1.

4.4. Synthesis of ionic liquid-modified MOF (NH_2–Fe MOF-IL)

A solution of NH_2–Fe MOF material (0.5 g), **IL** (2 mmol, 0.54 g), and Et_3N (3 mmol, 0.42 mL) were poured in a 500 mL flask containing DMF (2 mL) and stirred at 40 °C overnight. Then, the reaction mixture was subjected to centrifugation and resulting solid was washed several times with absolute ethanol, and dried at 40 °C for 12 hours in a vacuum oven.

4.5. Synthesis of Au@Fe-MOF-IL

The NH_2–Fe-MOF-IL material (0.5 g) was dispersed in DMF *via* 5 min sonication. In another flask, $HAuCl_4 \cdot 3H_2O$ (0.02 mmol, 8 mg) was dissolved in the DMF (2 mL) by sonication, then added dropwise to the MOF solution during 20 min. Then, a $NaBH_4$ solution (0.5 mmol, 19 mg in 2 mL DMF) was added dropwise and allowed to react at room temperature for 24 h. The reaction was submitted to centrifugation of the reaction mixture, followed by washing of resulting solid with DMF and absolute ethanol and drying at 40 °C for 24 h in a vacuum oven.

4.6. Synthesis of Pd@Fe-MOF-IL

NH_2–Fe-MOF-IL (0.5 g) was sonicated for 5 minutes in DMF. By sonication, $PdCl_2$ (0.07 mmol, 12.5 mg in 2 mL DMF) was dissolved in DMF (2 mL) and then added dropwise to the MOF solution for 20 minutes. In the end, the reaction mixture was

centrifuged, washed with DMF and absolute ethanol, and dried at 40 °C for 24 hours in a vacuum oven.

4.7. General procedure for the reduction of nitrophenols

A 5 mL glass flask was filled with nitrophenol (0.5 mmol), $NaBH_4$ (2 mmol), Au@Fe-MOF-IL catalyst (0.03 mol% Au, 2.1 mol% Fe, 6 mg), and H_2O (3 mL). Afterwards, the reaction mixture was continuously stirred at room temperature for the desired duration. TLC and GC were used to monitor the progress of the reactions. After the reaction was completed, distilled water and ethyl acetate were used to extract the crude product. In the end, the pure product was isolated using column or plate chromatography.

4.8. General strategy of nitrophenols reduction studied by UV-vis

The reaction mixture consists of a 2.5 mL aqueous solution of corresponding nitrophenol isomers (0.12 mM), a 0.5 mL aqueous solution of fresh $NaBH_4$ (0.5 mL, 0.5 M), and 1 mg Au@Fe-MOF-IL catalyst were poured into 5 mL reaction tube and mixture was stirred at room temperature. Following this, a portion of the reaction mixture was taken out, and its catalyst was separated from the suspension. The conversion of nitrophenol isomer to aminophenol, was measured by using a UV-vis spectrophotometer after filtering off the residues.

4.9. General strategy of dye reduction (MB, MO, and MR)

The aqueous solution of desired dye (MB, MO, or MR) (3 mL, 0.05 mM), an aqueous solution of fresh $NaBH_4$ (0.5 mL, 0.05 mM), and catalyst Au@Fe-MOF-IL (1 mg) were poured in a 5 mL flask, and the mixture was stirred at room temperature. Afterward, a portion of the reaction mixture taken out, and its catalyst separated from the suspension. Next, the residue was filtered off, and its corresponding UV-vis absorption spectrum was measured by a UV-vis spectrophotometer.

4.10. General method for the Sonogashira–Hagihara cross-coupling reaction

A 10 mL round-bottomed flask was charged with a mixture of aryl halide (0.5 mmol), Pd@Fe-MOF-IL catalyst (0.05 mol% Pd, 1.7 mol% Fe, 12.5 mg, for ArI, and 0.11 mol% Pd, 7.4 mol% Fe, 25 mg for ArBr), DABCO (0.75 mmol), and DMF (2 mL), and alkyne (0.8 mmol) under argon atmosphere. The reaction mixture was allowed to stir at 80 °C and progress of reaction was monitored by GC. After completing the reaction, the catalyst was removed by filtration and the residue diluted with water (6 mL), then the crude product was extracted with ethyl acetate (3 × 5 mL). Further purification was performed using column chromatography on silica gel using hexane and ethyl acetate as eluent.

Conflicts of interest

The authors declare no competing financial interest.

Acknowledgements

The authors are grateful to Institute for Advanced Studies in Basic Sciences (IASBS) Research Council, University of Alicante and Persian Gulf University. We also thank the continuous financial support from the Spanish Ministerio de Economía y Competitividad (MINECO; project CTQ2017-85093-P), Ministerio de Ciencia, Innovación y Universidades (RED2018-102387-T, PID2019-107268GB-100), FEDER, the Generalitat Valenciana (IDIFEDER/2021/013) and the University of Alicante (VIGROB-068).

Notes and references

1 A. G. Wong-Foy, A. J. Matzger and O. M. Yaghi, Exceptional H_2 Saturation Uptake in Microporous Metal-Organic Frameworks, *J. Am. Chem. Soc.*, 2006, **128**, 3494–3495.
2 C. J. Doonan, W. Morris, H. Furukawa and O. M. Yaghi, Isoreticular Metalation of Metal-Organic Frameworks, *J. Am. Chem. Soc.*, 2009, **131**, 9492–9493.
3 R. J. Kuppler, D. J. Timmons, Q.-R. Fang, J.-R. Li, T. A. Makal, M. D. Young, D. Yuan, D. Zhao, W. Zhuang and H.-C. Zhou, Potential Applications of Metal-Organic Frameworks, *Coord. Chem. Rev.*, 2009, **253**, 3042–3066.
4 M. Y. Masoomi, A. Morsali, A. Dhakshinamoorthy and H. Garcia, Mixed-Metal MOFs: Unique Opportunities in Metal-Organic Framework (MOF) Functionality and Design, *Angew. Chem., Int. Ed.*, 2019, **131**, 15330–15347.
5 H.-Y. Li, S.-N. Zhao, S.-Q. Zang and J. Li, Functional Metal-Organic Frameworks as Effective Sensors of Gases and Volatile Compounds, *Chem. Soc. Rev.*, 2020, **49**, 6364–6401.
6 Q. Bi, Q. Ma, K. Tao and L. Han, Hierarchical core–shell 2D MOF nanosheet hybrid arrays for high-performance hybrid supercapacitors, *Dalton Trans.*, 2021, **50**, 8179–8188.
7 X. Zhang, Z. Chen, X. Liu, S. L. Hanna, X. Wang, R. Taheri-Ledari, A. Maleki, P. Li and O. K. Farha, A historical overview of the activation and porosity of metal–organic frameworks, *Chem. Soc. Rev.*, 2020, **49**, 7406–7427.
8 D. Li, H.-Q. Xu, L. Jiao and H.-L. Jiang, Metal-Organic Frameworks for Catalysis: State of the Art, Challenges, and Opportunities, *EnergyChem*, 2019, **1**, 100005.
9 A. Das, N. Anbu, A. Dhakshinamoorthy and S. Biswas, A Highly Catalytically Active Hf(IV) Metal-Organic Framework for Knoevenagel Condensation, *Microporous Mesoporous Mater.*, 2019, **284**, 459–467.
10 D. Jiang, T. Mallat, F. Krumeich and A. Baiker, Copper-Based Metal-Organic Framework for the Facile Ring-Opening of Epoxides, *J. Catal.*, 2008, **257**, 390–395.
11 K. M. Jablonka, D. Ongari, S. M. Moosavi and B. Smit, Using Collective Knowledge to Assign Oxidation States of Metal Cations in Metal-Organic Frameworks, *Nat. Chem.*, 2021, **13**, 771–777.
12 S. M. Cohen, Postsynthetic Methods for the Functionalization of Metal-Organic Frameworks, *Chem. Rev.*, 2012, **112**, 970–1000.
13 K. K. Tanabe and S. M. Cohen, Postsynthetic Modification of Metal-Organic Frameworks-A Progress Report, *Chem. Soc. Rev.*, 2011, **40**, 498–519.

14 K. K. Tanabe, Z. Wang and S. M. Cohen, Systematic Functionalization of a Metal-Organic Framework *via* a Postsynthetic Modification Approach, *J. Am. Chem. Soc.*, 2008, **130**, 8508–8517.

15 Y. Xin-Yue, G. Li, S. Ya-Ming, Z. Wen-Jie, G.-Q. Xiang, X.-M. Jiang, H. Li-Jun and S.-S. Zhang, Preparation of Ionic Liquids-Modified Metal Organic Frameworks Composite Materials and Their Application in Separation Analysis, *Chin. J. Anal. Chem.*, 2020, **48**, 1607–1615.

16 M. Gholinejad, Z. Naghshbandi and J. M. Sansano, Zeolitic Imidazolate Frameworks-67 (ZIF-67) Supported PdCu Nanoparticles for Enhanced Catalytic Activity in Sonogashira-Hagihara and Nitro Group Reduction under Mild Conditions, *Mol. Catal.*, 2022, **518**, 112093.

17 F. Khosravi, M. Gholinejad, J. M. Sansano and R. Luque, Bimetallic Fe–Cu Metal Organic Frameworks for Room Temperature Catalysis, *Appl. Organomet. Chem.*, 2022, **36**, e6749.

18 A. Aijaz, A. Karkamkar, Y. J. Choi, N. Tsumori, E. Rönnebro, T. Autrey, H. Shioyama and Q. Xu, Immobilizing Highly Catalytically Active Pt Nanoparticles Inside the Pores of Metal-Organic Framework: A Double Solvents Approach, *J. Am. Chem. Soc.*, 2012, **134**, 13926–13929.

19 M. Ikram, E. Umar, A. Raza, A. Haider, S. Naz, D. A. Ul-Hamid, J. Haider, I. Shahzadi, J. Hassan and S. Ali, Dye Degradation Performance, Bactericidal Behavior and Molecular Docking Analysis of Cu-Doped TiO_2 Nanoparticles, *RSC Adv.*, 2020, **10**, 24215–24233.

20 J. Li, Q. Liu, Q. Ji and B. Lai, Degradation of *p*-Nitrophenol (PNP) in Aqueous Solution by Fe^0-PM-PS System through Response Surface Methodology (RSM), *Appl. Catal., B*, 2017, **200**, 633–646.

21 M. Orlandi, D. Brenna, R. Harms, S. Jost and M. Benaglia, Recent Developments in the Reduction of Aromatic and Aliphatic Nitro Compounds to Amines, *Org. Process Res. Dev.*, 2016, **22**, 430–445.

22 P. C. Lindholm-Lehto, J. S. Knuutinen, H. S. J. Ahkola and S. H. Herve, Refractory Organic Pollutants and Toxicity in Pulp and Paper Mill Wastewaters, *Environ. Sci. Pollut. Res.*, 2015, **22**, 6473–6499.

23 S. Haider, T. Kamal, S. B. Khan, M. Omer, A. Haider, F. U. Khan and A. M. Asiri, Natural Polymers Supported Copper Nanoparticles for Pollutants Degradation, *Appl. Surf. Sci.*, 2016, **387**, 1154–1161.

24 S. Gul, Z. A. Rehan, S. A. Khan, K. Akhtar, M. A. Khan, M. I. Khan, M. I. Rashid, A. M. Asiri and S. B. Khan, Antibacterial PES-CA-Ag_2O Nanocomposite Supported Cu Nanoparticles Membrane toward Ultrafiltration, BSA Rejection and Reduction of Nitrophenol, *J. Mol. Liq.*, 2017, **230**, 616–624.

25 N. T. Tavengwa, E. Cukrowska and L. Chimuka, Application of Magnetic Molecularly Imprinted Polymers for the Solid Phase Extraction of Selected Nitroaromatic Compounds from Contaminated Aqueous Environments, *Sep. Sci. Technol.*, 2017, **52**, 467–475.

26 A. Boehncke, I. Mangelsdorf, A. Wibbertmann, World Health Organization and International Programme on Chemical Safety, *Mononitrophenols*, World Health Organization, 2000.

27 T. Cattoor, European Legislation Relating to Textile Dyeing, *Environmental Aspects of Textile Dyeing*, CRC Press, Cambridge (UK), 2007, pp. 1–29.

28 *Environmental Aspects of Textile Dyeing*, ed. R. Christie, CRC Press, Cambridge (UK), 2007.

29 J. Michałowicz and W. Duda, Phenols-Sources and Toxicity, *Pol. J. Environ. Stud.*, 2007, **16**, 347–362.

30 H. Zhang, K. Taya, K. Nagaoka, M. Yoshida and G. Watanabe, 4-Nitrophenol (PNP) Inhibits the Expression of Estrogen Receptor β and Disrupts Steroidogenesis During the Ovarian Development in Female Rats, *Environ. Pollut.*, 2017, **229**, 1–9.

31 V. Belessi, G. Romanos, N. Boukos, D. Lambropoulou and C. Trapalis, Removal of Reactive Red 195 from Aqueous Solutions by Adsorption on the Surface of TiO_2 Nanoparticles, *J. Hazard. Mater.*, 2009, **170**, 836–844.

32 S. A. Khan, S. B. Khan and A. M. Asiri, Toward the Design of Zn–Al and Zn–Cr LDH Wrapped in Activated Carbon for the Solar Assisted De-Coloration of Organic Dyes, *RSC Adv.*, 2016, **6**, 83196–83208.

33 E. J. Roberts, L. R. Karadaghi, L. Wang, N. Malmstadt and R. L. Brutchey, Continuous Flow Methods of Fabricating Catalytically Active Metal Nanoparticles, *ACS Appl. Mater. Interfaces*, 2019, **11**, 27479–27502.

34 M. Soltani and M. Zabihi, Hydrogen Generation by Catalytic Hydrolysis of Sodium Borohydride Using the Nano-Bimetallic Catalysts Supported on the Core-Shell Magnetic Nanocomposite of Activated Carbon, *Int. J. Hydrogen Energy*, 2020, **45**, 12331–12346.

35 N. Zhang, C. Xue, K. Wang and Z. Fang, Efficient Oxidative Degradation of Fluconazole by a Heterogeneous Fenton Process with Cu-V Bimetallic Catalysts, *Chem. Eng. J.*, 2020, **380**, 122516.

36 S. Frigoli, C. Fuganti, L. Malpezzi and S. Serra, A Practical and Efficient Process for the Preparation of Tazarotene, *Org. Process Res. Dev.*, 2005, **9**, 646–650.

37 M. C. Bagley, J. W. Dale, E. A. Merritt and X. Xiong, Thiopeptide Antibiotics, *Chem. Rev.*, 2005, **105**, 685–714.

38 R. Chinchilla and C. Nájera, The Sonogashira Reaction: A Booming Methodology in Synthetic Organic Chemistry, *Chem. Rev.*, 2007, **107**, 874–922.

39 M. Karak, L. C. A. Barbosa and G. C. Hargaden, Recent Mechanistic Developments and Next Generation Catalysts for the Sonogashira Coupling Reaction, *RSC Adv.*, 2014, **4**, 53442–53466.

40 A. M. Thomas, A. Sujatha and G. Anilkumar, Recent Advances and Perspectives in Copper-Catalyzed Sonogashira Coupling Reactions, *RSC Adv.*, 2014, **4**, 21688–21698.

41 F. Mohajer, M. M. Heravi, V. Zadsirjan and N. Poormohammad, Copper-Free Sonogashira Cross-Coupling Reactions: An Overview, *RSC Adv.*, 2021, **11**, 6885–6925.

42 X. Yue, W. Guo, X. Li, H. Zhou and R. Wang, Core-Shell Fe_3O_4@MIL-101(Fe) Composites as Heterogeneous Catalysts of Persulfate Activation for the Removal of Acid Orange 7, *Environ. Sci. Pollut. Res.*, 2016, **23**, 15218–15226.

43 S. Handa, Y. Wang, F. Gallou and B. H. Lipshutz, Sustainable Fe–ppm Pd Nanoparticle Catalysis of Suzuki-Miyaura Cross-Couplings in Water, *Science*, 2015, **349**, 1087–1091.

44 A. B. Wood, S. Plummer, R. I. Robinson, M. Smith, J. Chang, F. Gallou and B. H. Lipshutz, Continuous Slurry Plug Flow Fe/ppm Pd Nanoparticle-Catalyzed Suzuki–Miyaura Couplings in Water Utilizing Novel Solid Handling Equipment, *Green Chem.*, 2021, **23**, 7724–7730.

45 Y. Hu, M. J. Wong and B. H. Lipshutz, ppm Pd-Containing Nanoparticles as Catalysts for Negishi Couplings … in Water, *Angew. Chem., Int. Ed.*, 2022, **134**, e202209784.

46 M. Carril, A. Correa and C. Bolm, Iron-catalyzed Sonogashira reactions, *Angew. Chem., Int. Ed.*, 2008, **47**, 4862–4865.

47 S. L. Buchwald and C. Bolm, On the role of metal contaminants in catalyses with $FeCl_3$, *Angew. Chem.*, 2009, **121**, 5694–5695.

48 M. Martis, K. Mori, K. Fujiwara, W.-S. Ahn and H. Yamashita, Amine-Functionalized MIL-125 with Imbedded Palladium Nanoparticles as an Efficient Catalyst for Dehydrogenation of Formic Acid at Ambient Temperature, *J. Phys. Chem. C*, 2013, **117**, 22805–22810.

49 N. D. McNamara, G. T. Neumann, E. T. Masko, J. A. Urban and J. C. Hicks, Catalytic Performance and Stability of (V MIL-47) and (Ti MIL-125) in the Oxidative Desulfurization of Heterocyclic Aromatic Sulfur Compounds, *J. Catal.*, 2013, **305**, 217–226.

50 S. Wang, W. Deng, L. Yang, Y. Tan, Q. Xie and S. Yao, Copper-Based Metal–Organic Framework Nanoparticles with Peroxidase-Like Activity for Sensitive Colorimetric Detection of *Staphylococcus aureus*, *ACS Appl. Mater. Interfaces*, 2017, **9**, 24440–24445.

51 J. Sun, G. Yu, Q. Huo, Q. Kan and J. Guan, Epoxidation of Styrene Over Fe(Cr-MIL-101) Metal-Organic Frameworks, *RSC Adv.*, 2014, **4**, 38048–38054.

52 B. C. e. Silva, K. Irikura, R. C. G. Frem and M. V. B. Zanoni, Effect of Cu(BDC-NH_2) MOF Deposited on Cu/Cu_2O Electrode and Its Better Performance in Photoelectrocatalytic Reduction of CO_2, *J. Electroanal. Chem.*, 2021, **880**, 114856.

53 B. Iqbal, M. Saleem, S. N. Arshad, J. Rashid, N. Hussain and M. Zaheer, One-Pot Synthesis of Heterobimetallic Metal-Organic Frameworks (MOFs) for Multifunctional Catalysis, *Chem.–Eur. J.*, 2019, **25**, 10490–10498.

54 A. G. Kuba, Y. Y. Smolin, M. Soroush and K. K. Lau, Synthesis and Integration of Poly(1-Vinylimidazole) Polymer Electrolyte in Dye Sensitized Solar Cells by Initiated Chemical Vapor Deposition, *Chem. Eng. Sci.*, 2016, **154**, 136–142.

55 I. A. Lawal, M. M. Lawal, S. O. Akpotu, M. A. Azeez, P. Ndungu and B. Moodley, Theoretical and Experimental Adsorption Studies of Sulfamethoxazole and Ketoprofen on Synthesized Ionic Liquids Modified CNTs, *Ecotoxicol. Environ. Saf.*, 2018, **161**, 542–552.

56 L. Shao, Z. Yu, X. Li, X. Li, H. Zeng and X. Feng, Carbon Nanodots Anchored Onto the Metal-Organic Framework NH_2-MIL-88B(Fe) as a Novel Visible Light-Driven Photocatalyst: Photocatalytic Performance and Mechanism Investigation, *Appl. Surf. Sci.*, 2020, **505**, 144616.

57 C. Xu, M. Bao, J. Ren and Z. Zhang, NH_2-MIL-88B ($Fe_\alpha In_{1-\alpha}$) Mixed-MOFs Designed for Enhancing Photocatalytic Cr(VI) Reduction and Tetracycline Elimination, *RSC Adv.*, 2020, **10**, 39080–39086.

58 L. Zeng, X. Li, S. Fan, M. Zhang, Z. Yin, M. Tadé and S. Liu, Photo-Driven Bioelectrochemical Photocathode with Polydopamine-Coated TiO_2 Nanotubes for Self-Sustaining MoS_2 Synthesis to Facilitate Hydrogen Evolution, *J. Power Sources*, 2019, **413**, 310–317.

59 S. Gao, N. Zhao, M. Shu and S. Che, Palladium Nanoparticles Supported on MOF-5: A Highly Active Catalyst for a Ligand- and Copper-Free Sonogashira Coupling Reaction, *Appl. Catal., A*, 2010, **38**, 196–201.

60 Y. Wu, Y. Xiao, H. Yuan, Z. Zhang, S. Shi, R. Wei, L. Gao and G. Xiao, Imidazolium Ionic Liquid Functionalized UiO-66-NH_2 as Highly Efficient Catalysts for Chemical Fixation of CO_2 Into Cyclic Carbonates, *Microporous Mesoporous Mater.*, 2021, **310**, 110578.

61 H. Zhu, J. Wu, M. Fang, L. Tan, C. Chen, N. S. Alharbi, T. Hayat and X. Tan, Synthesis of a Core–Shell Magnetic Fe_3O_4–NH_2@PmPD Nanocomposite for Efficient Removal of Cr(VI) From Aqueous Media, *RSC Adv.*, 2017, **7**, 36231–36241.

62 E. Mazzotta, S. Rella, A. Turco and C. Malitesta, XPS in Development of Chemical Sensors, *RSC Adv.*, 2015, **5**, 83164–83186.

63 X. Yi, X. He, F. Yin, T. Yang, B. Chen and G. Li, NH_2-MIL-88B–Fe for Electrocatalytic N_2 Fixation to NH_3 with High Faradaic Efficiency under Ambient Conditions in Neutral Electrolyte, *J. Mater. Sci.*, 2020, **55**, 12041–12052.

64 F. Al-Wadaani, A. Omer, M. Abboudi, H. Oudghiri Hassani, S. Rakass, M. Messali and M. Benaissa, High catalytic efficiency of nanostructured β-$CoMoO_4$ in the reduction of the ortho-, meta-and para-nitrophenol isomers, *Molecules*, 2018, **23**, 364.

65 Y. Xu, X. Shi, R. Hua, R. Zhang, Y. Yao, B. Zhao, T. Liu, J. Zheng and G. Lu, Remarkably Catalytic Activity in Reduction of 4-Nitrophenol and Methylene Blue by Fe_3O_4@COF Supported Noble Metal Nanoparticles, *Appl. Catal., B*, 2020, **260**, 118142.

66 L. Ayed, A. Mahdhi, A. Cheref and A. Bakhrouf, Decolorization and Degradation of Azo Dye Methyl Red by an Isolated *Sphingomonas paucimobilis*: Biotoxicity and Metabolites Characterization, *Desalination*, 2011, **274**, 272–277.

67 P. Kumar, M. Govindaraju, S. Senthamilselvi and K. Premkumar, Photocatalytic Degradation of Methyl Orange Dye Using Silver (Ag) Nanoparticles Synthesized from Ulva Lactuca, *Colloids Surf., B*, 2013, **103**, 658–661.

68 F. Khosravi, M. Gholinejad, J. M. Sansano and R. Luque, Low-Amount Palladium Supported on Fe-Cu MOF: Synergetic Effect Between Pd, Cu and Fe in Sonogashira-Hagihara Coupling Reaction and Reduction of Organic Dyes, *Mol. Catal.*, 2022, **522**, 112199.